Supporting Information

MgO passivation layer and hydrotalcite derived spinel Co_2AlO_4 synergically promote photoelectrochemical water oxidation conducted by $BiVO_4$-based photoanode

Jing Zhang [a], Kaiyi Chen [b], Yan Bai [a], Lei Wang [a], Jingwei Huang [a], Houde She [a], Qizhao Wang *[a,b]

[a] *College of Chemistry and Chemical Engineering, Northwest Normal University, Lanzhou 730070, China*
[b] *School of Water and Environment, Key Laboratory of Subsurface Hydrology and Ecological Effects in Arid Region of Ministry of Education, Chang'an University, Xi'an 710054, China.*

[c] *College of Geography and Environmental Science, Northwest Normal University, Lanzhou 730070, China*

*Corresponding authors. Tel: +86 931 7972677; Fax: +86 931 7972677.
*Corresponding authors.
E-mail: wangqizhao@163.com, qizhaosjtu@gmail.com (Q. Wang)

1. Chemicals

$Co(NO_3)_2·6H_2O$, $Al(NO_3)_3·9H_2O$, $CO(NH_2)_2$, $Bi(NO_3)_3·5H_2O$, NaOH, KI, and absolute ethanol were purchased from Sinopharm Chemical Reagent Co., Ltd. NH_4F was provided by Yantai Shuangshuang Chemical Co., Ltd. $Mg(NO_3)_2·6H_2O$ was purchased from Tianjin Kaixin Chemical Industry Co., Ltd. The FTO conductive glass was provided by Zhuhai Kaiwei Photoelectric Technology Co., Ltd. The above reagents are analytical grade and do not require purification.

2. Preparation of $BiVO_4$ photoanode

First, the pH of 0.4 M KI (50 mL) solution was adjusted to 1.6 with HNO_3, then 0.970 g $Bi(NO_3)_3·5H_2O$ was added to stir and dissolve, and mixed with 0.23 M p-benzoquinone ethanol solution (20 mL) to obtain BiOI precursor solution. Using a three-electrode system, cyclic voltammetry (CV) deposition in the potential range of -0.13 V ~ 0 V, scanning rate of 5 mV/s. Then, rinse it with deionized water and dry. 100 μL of 0.2 M $VO(acac)_2$ solution was dropped on the surface of BiOI and heated at a rate of 2 °C /min in muffle furnace 450 °C for 2 h. Then the residual V_2O_5 on the surface was removed with 1 M NaOH solution to obtain $BiVO_4$ electrode.

3. Characterizations and PEC measurements

The structure of the samples was characterized by X-ray diffractometer (XRD, X-Pert PRO MPD). X-ray photoelectron spectroscopy (ESCALAB Xi^+) analyzes the elemental composition and surface state of the samples. SEM (Hitachi S4800) and TEM (JEM-2100, JEOL, Japan) were used to observe the morphology and microstructures of electrodes. The absorbance of the electrodes was measured by UV-Vis diffuse reflectance (Shimadzu UV-3600 Plus). The fluorescence absorption of the electrodes was measured using a spectrophotometer (PL, Shimadzu. PELS-55).

All photoelectrochemical performance tests were performed using a CHI 660D electrochemical workstation (Shanghai Chenhua Instrument Co., Ltd.). Xenon lamp (PLS-SXE300C) simulated AM 1.5G illumination (100 mW cm^{-2}) with 0.5 M Na_2SO_4 (pH=7) as the electrolyte solution. The incident photon-to-current efficiency (IPCE) test was done using a xenon lamp equipped with a monochromator (71SWS, Beijing

NBeT Technology Co., Ltd.). Gas chromatography (GC-9560) detects the evolved gases.

All electric potentials were converted with the following formula:

$$E_{RHE} = 0.197 + 0.059 \times pH + E^{\theta}_{Ag/AgCl}$$

The incident photon-to-current efficiency (IPCE) calculation formula is as follows:

$$IPCE = (1240 \times J)/ (\lambda \times P)$$

Where J (mA cm^{-2}) is the current density measured at each specific wavelength, λ (nm) is the wavelength of incident light, and P is the power density of the incident light at a special wavelength.

The absorbed photon-to-current efficiency (APCE) is derived from the IPCE and light harvesting efficiency (LHE) by using the following formula:

$$APCE = IPCE/LHE$$

$$LHE = 1\text{-}10^{-A}(\lambda)$$ (A is the absorbance at a special wavelength λ)

The applied bias photon-current efficiency (ABPE) is calculated according to the following formula:

$$ABPE = [J \times (1.23 - V_{app})]/P_{light}$$

Where J is the photocurrent density (mA cm^{-2}), V_{app} is the applied bias voltage (vs RHE), and P_{light} is the incident light intensity of 100 mW cm^{-2} (AM 1.5 G).

The carrier concentration of photoanodes is calculated by the following formula:

$$N_d = \left(\frac{2}{q\varepsilon\varepsilon_0}\right) \times \left[\frac{d(\frac{1}{c^2})}{dv}\right]^{-1}$$

Where q is the electron charge, the dielectric constant of the semiconductor ($BiVO_4$ = 68), ε_0 the vacuum dielectric constant, c is capacitance and v is plus voltage.

4. Description of DFT calculation

All calculations are based on density functional theory (DFT) using Vienna Ab initio Simulation Package (VASP). The generalized gradient approximation (GGA) and Perdew-Burke-Ernzerhof (PBE) were used to describe the exchange-correlation energy. MgO (222), $BiVO_4$ (121), and MgO/$BiVO_4$ were modeled as plates with a vacuum spacing of 15 Å along the Z direction, and the Brillouin zone was sampled

using a Gamma-center k-point mesh. The K point of 4×4×1 was used for geometric optimization. The plane wave cutoff for electronic wave functions was set to 520 eV. The convergence standard of energy and force during geometric structure optimization were 1.0×10^{-4} eV/atom and 0.02 eV/Å, respectively. For DOS calculation, the convergence standard of energy and force during geometric structure optimization were 1.0×10^{-4} eV/atom and 0.02 eV/Å and the K point is 4×4×4.

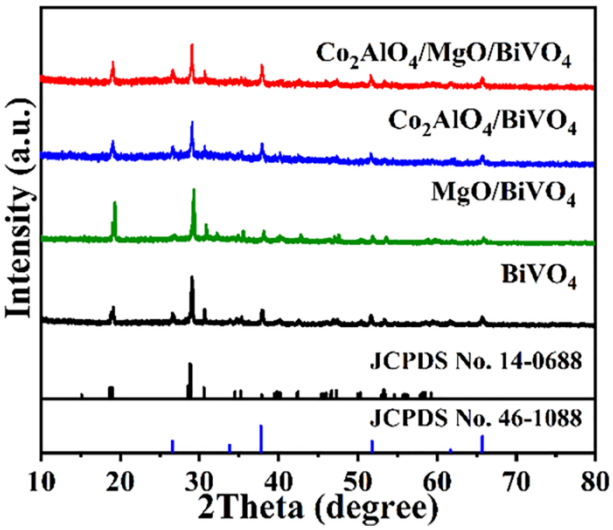

Fig. S1. XRD pattern of photoanodes.

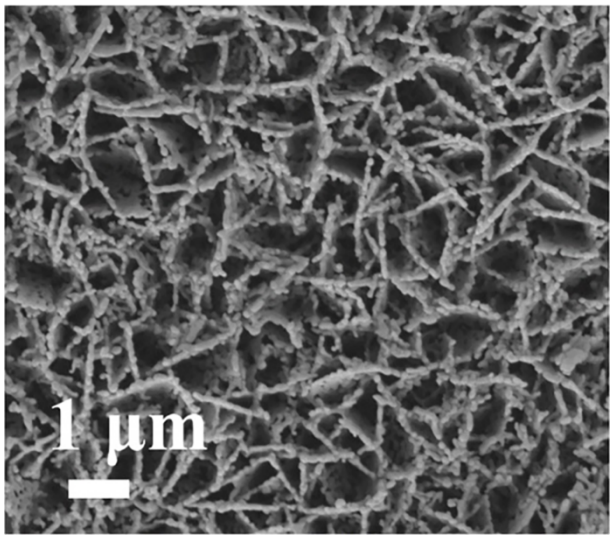

Fig. S2. SEM image of BiOI electrode.

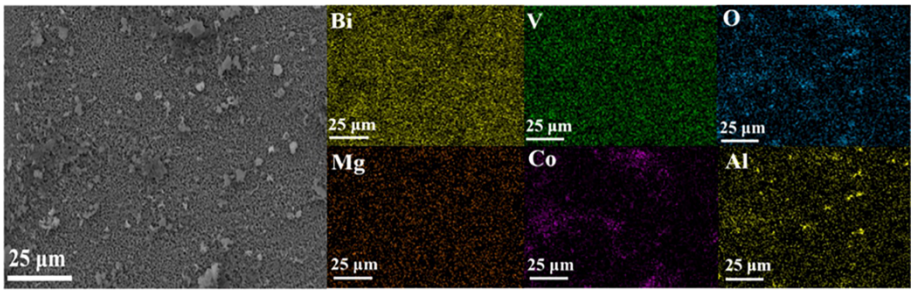

Fig. S3. The SEM-EDS mapping of Co_2AlO_4/MgO/$BiVO_4$ electrode.

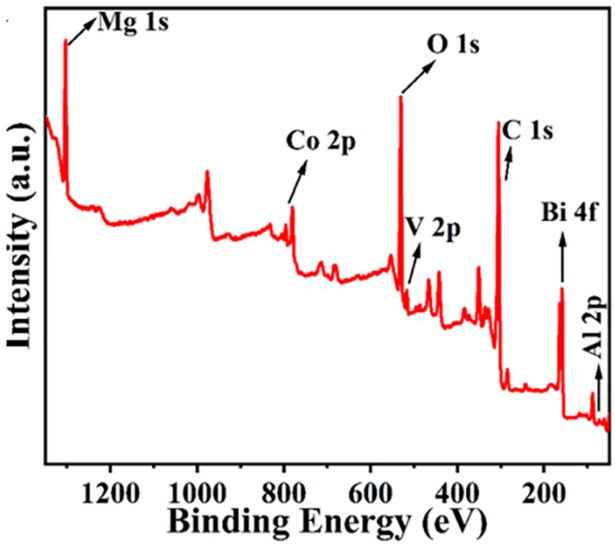

Fig. S4. Full range XPS spectra of Co_2AlO_4/ MgO/$BiVO_4$.

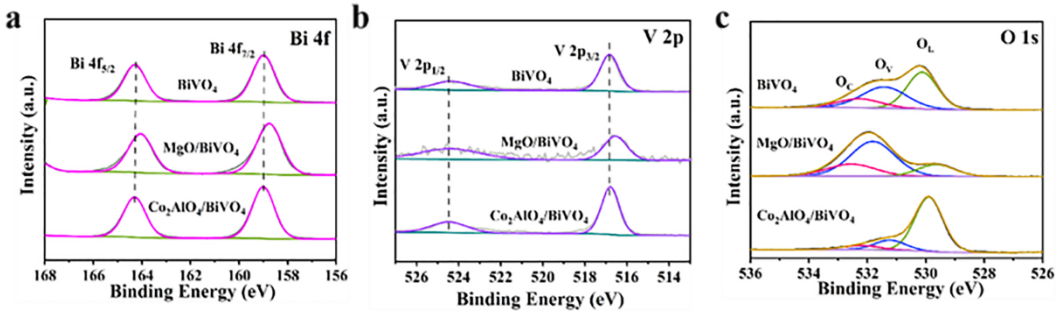

Fig. S5. Bi 4f (a), V 2p (b), and O 1s (c) XPS of $BiVO_4$, $MgO/BiVO_4$ and $Co_2AlO_4/BiVO_4$.

The peaks of Bi $4f_{7/2}$ and Bi $4f_{5/2}$ in $BiVO_4$ are located at 159.0 eV and 164.3 eV respectively. After the deposition of MgO, the two peaks were slightly shifted to a lower binding energy of about 0.1 eV, and the two peaks of $Co_2AlO_4/BiVO_4$ were not significantly shifted (Fig. S5a). Similarly, the peaks of V $2p_{3/2}$ and V $2p_{1/2}$ also vary slightly (Fig. S5b). The O 1s of $BiVO_4$ can be well synthesized into three peaks located at 530.1 eV, 531.4 eV and 532.4 eV, corresponding to lattice oxygen (O_L), oxygen vacancy adsorbed oxygen (O_V) and chemisorbed oxygen (Oc), respectively (Fig. S5c). It can be seen from the figure that the peaks of $MgO/BiVO_4$ and $Co_2AlO_4/BiVO_4$ are also slightly offset, and the O_V peak area in $MgO/BiVO_4$ accounts for a large proportion, so it can be inferred that the MgO passivation layer contributes part of the oxygen vacancy defect active site.

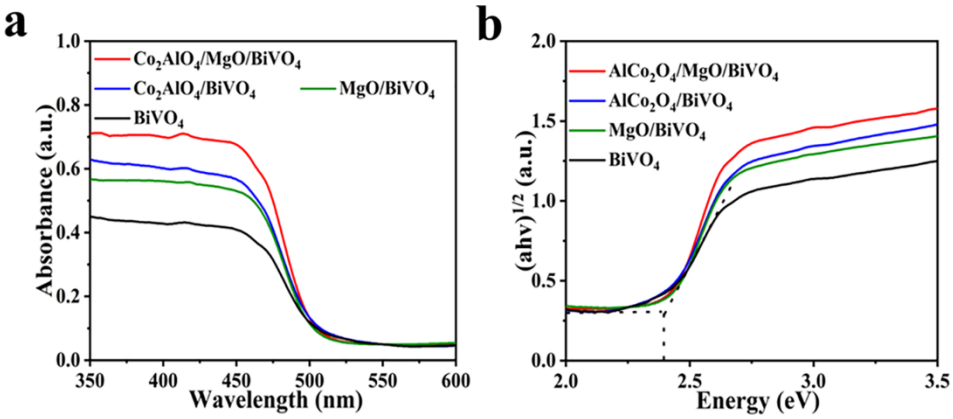

Fig. S6. UV–vis diffused reflectance (a) and the energy band gap spectra (b).

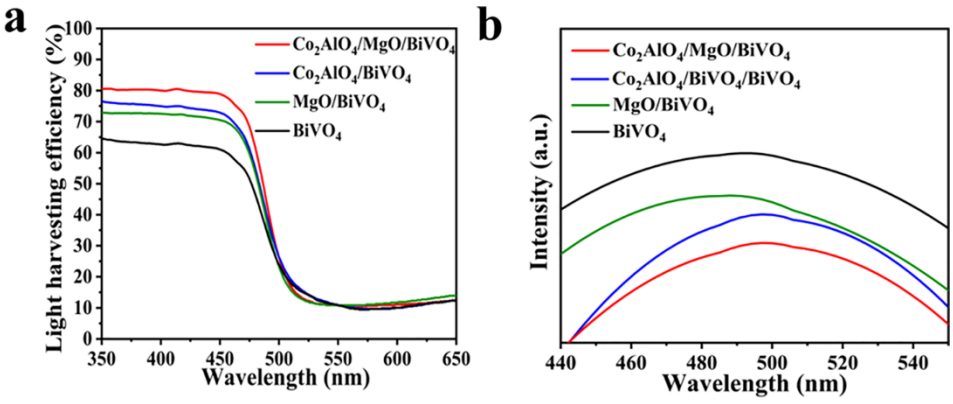

Fig. S7. Light harvesting efficiency (LHE) (a) and PL spectra of photoanodes at the emission wavelength (~350 nm) (b).

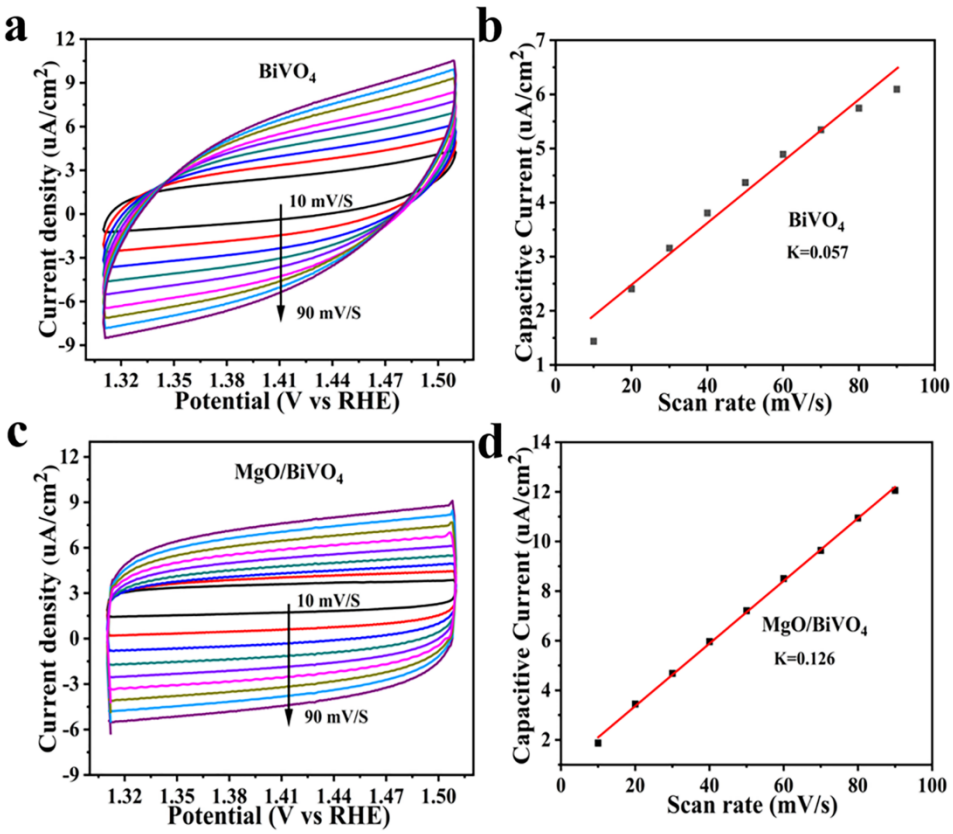

Fig. S8. The CV curves (a) and Cdl (b) diagrams of $BiVO_4$. The CV curves (c) and Cdl (d) diagrams of $MgO/BiVO_4$.

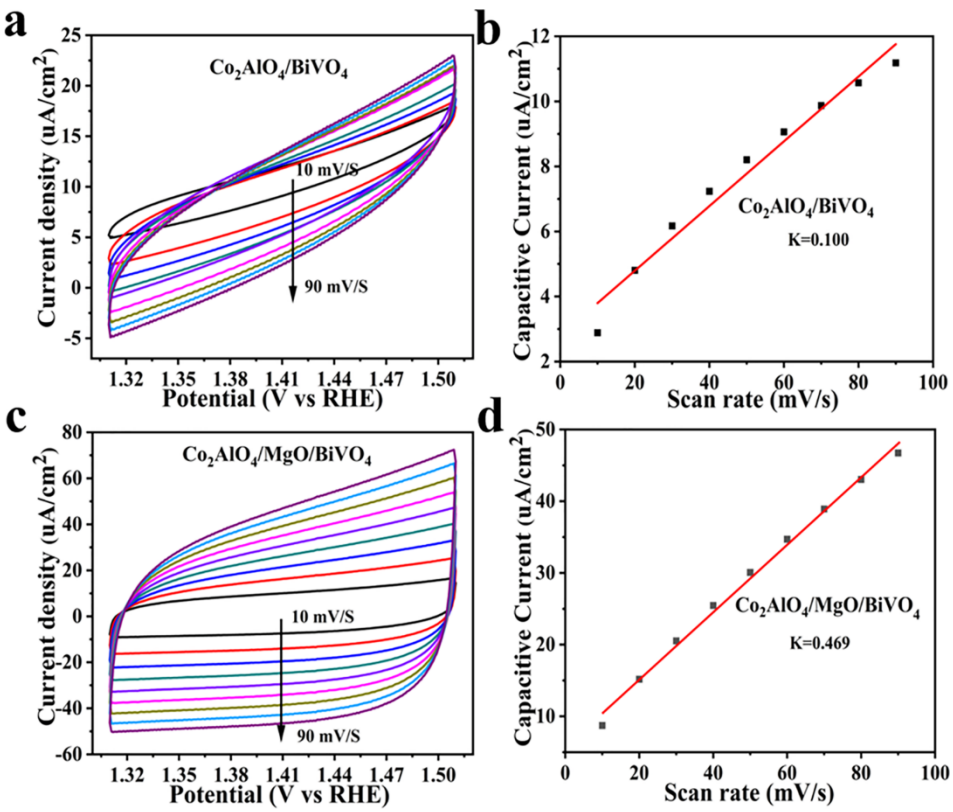

Fig. S9. The CV curves (a) and Cdl (b) diagrams of $Co_2AlO_4/BiVO_4$. The CV curves (c) and Cdl (d) diagrams of $Co_2AlO_4/MgO/BiVO_4$.

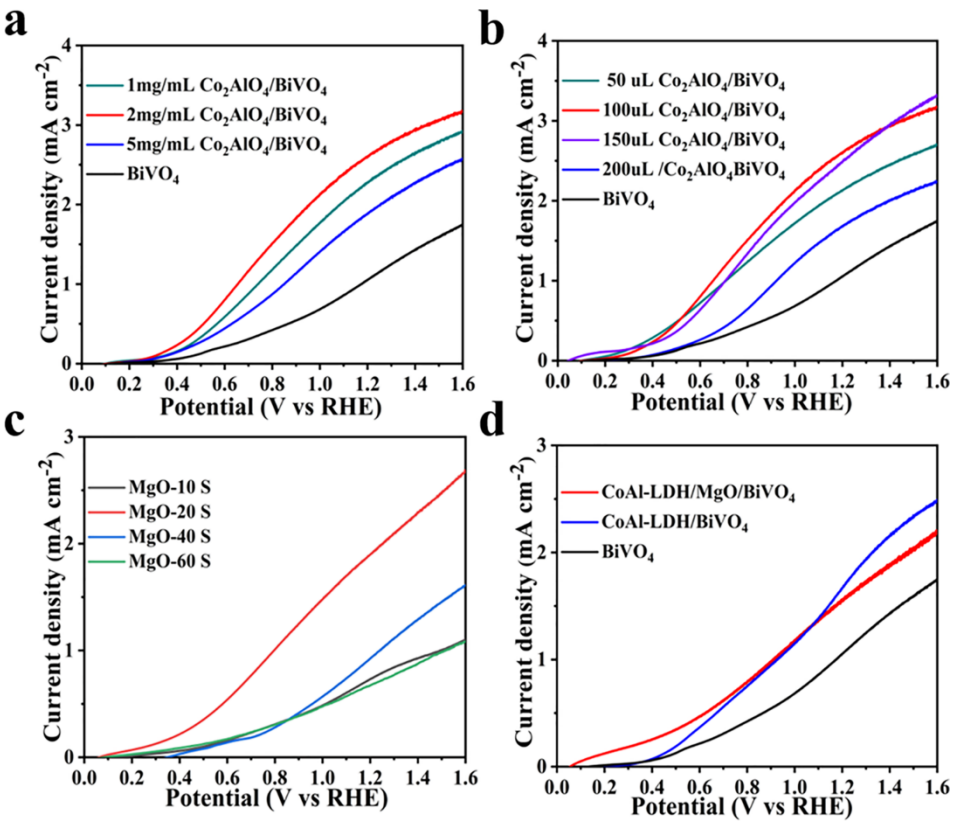

Fig. S10. The LSV curves are to regulate Co_2AlO_4 concentration (a), Co_2AlO_4 volume (b), MgO deposition time (c) and CoAl-LDH, respectively (d). All measurements were made in 0.5 M Na_2SO_4 (pH = 7) electrolyte under AM 1.5 G illumination.

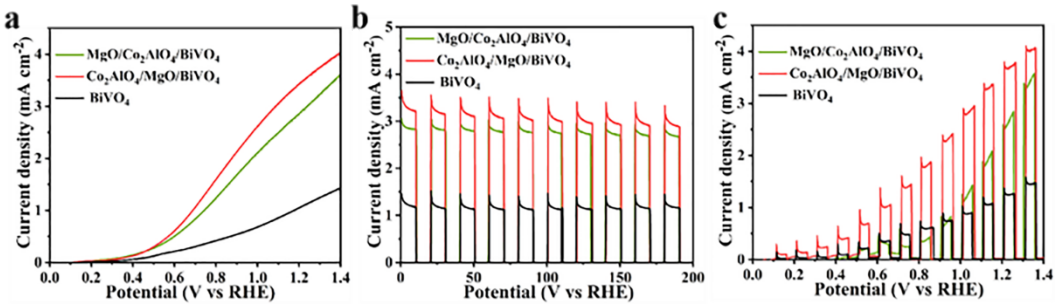

Fig. S11. LSV curves of photoanodes (a). I-t curves (b) and LSV chopped transient photocurrent curve of photoanodes in 0.5 M Na_2SO_4 (c).

Fig. S11a shows that the photocurrent density of $MgO/Co_2AlO_4/BiVO_4$ is 2.97 mA cm^{-2}, which is significantly higher than that of naked $BiVO_4$ (1.11 mA cm^{-2}). However, the photocurrent density of $Co_2AlO_4/MgO/BiVO_4$ is 3.52 mA cm^{-2} (1.23 V vs RHE). The photoanodes have good photoresponse and little attenuation of the curve (Fig. S11b). Fig. S11c shows the LSV curve of electrodes under chopped light irradiation, all electrodes exhibit a photocurrent consistent with Fig. S11a. The above test results show that $Co_2AlO_4/MgO/BiVO_4$ maximizes photoelectric performance.

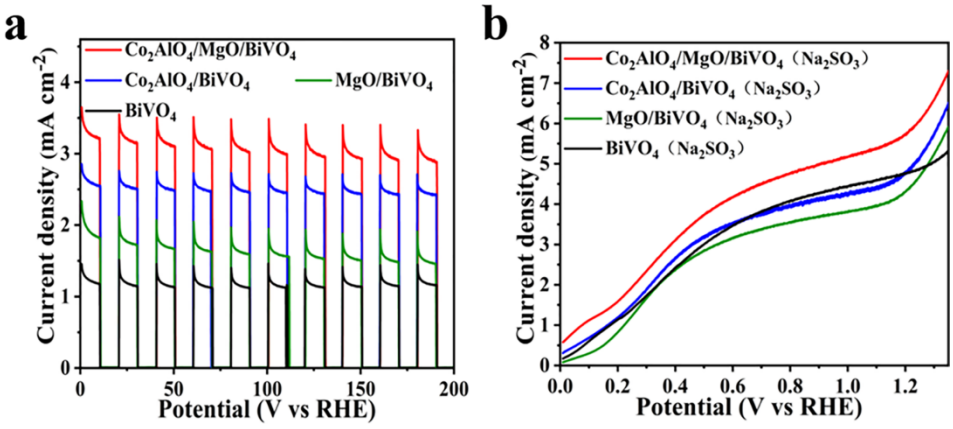

Fig. S12. I-t curves of electrodes in 0.5 M Na_2SO_4 (a). LSV curve of photoanodes with 1 M Na_2SO_3 in 0.5 M Na_2SO_4 under AM 1.5 G irradiation (b).

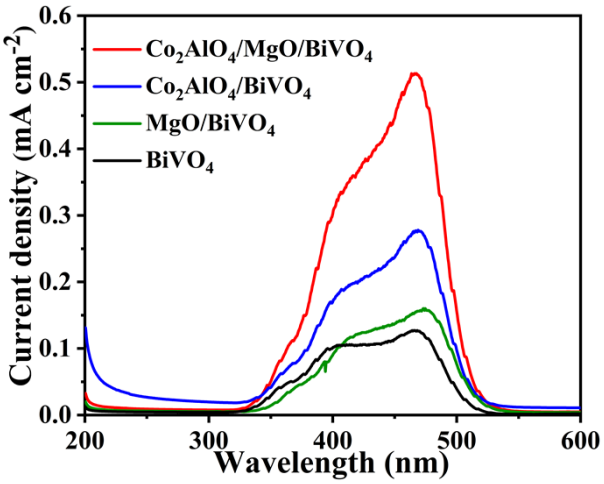

Fig. S13. Photocurrent density curves of photoanodes (350-600 nm).

The photocurrent density in the wavelength range of 350-600 nm was tested. It can be seen that Co_2AlO_4/MgO/$BiVO_4$ has the best photoelectric response (0.513 mA cm^{-2}) at about 467 nm, which is 4.0 times higher than that of $BiVO_4$ (0.127 mA cm^{-2}). It is further shown that the introduction of MgO passivation layer and Co_2AlO_4 can enhance the light absorption capacity and photocurrent conversion efficiency of the composite electrode.

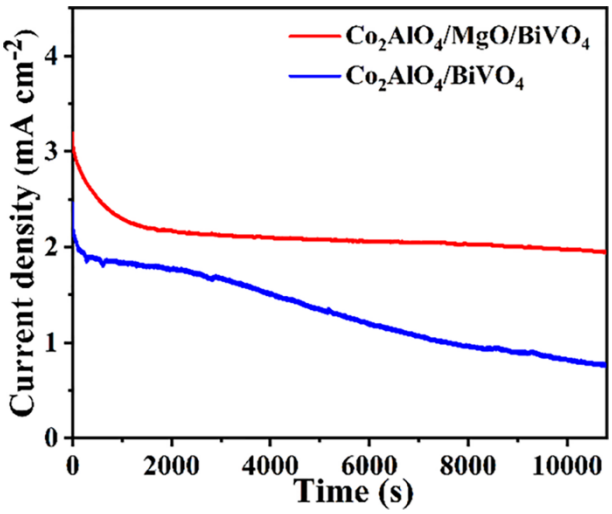

Fig. S14. Photocurrent density versus time curves of Co_2AlO_4/$BiVO_4$ and Co_2AlO_4/MgO/$BiVO_4$.

Table. S1. The charge transfer resistance (R_{ct}) of $BiVO_4$, $MgO/BiVO_4$, $Co_2AlO_4/BiVO_4$ and $Co_2AlO_4/MgO/BiVO_4$.

Sample	R_{ct} (Ω)
$Co_2AlO_4/MgO/BiVO_4$	146.4
$Co_2AlO_4/BiVO_4$	157.2
$MgO/BiVO_4$	257.5
$BiVO_4$	260.7

Table. S2. Carrier concentration (N_d) of $BiVO_4$, $MgO/BiVO_4$, $Co_2AlO_4/BiVO_4$ and $Co_2AlO_4/MgO/BiVO_4$.

Sample	N_d (cm^{-3})
$Co_2AlO_4/MgO/BiVO_4$	5.75338×10^{30}
$Co_2AlO_4/BiVO_4$	2.35107×10^{30}
$MgO/BiVO_4$	2.13158×10^{30}
$BiVO_4$	1.11577×10^{30}

Table. S3. Comparison of our work with previously reported the $BiVO_4$ photoanodes for PEC water oxidation under AM 1.5G (100 mW cm^{-2}) illumination.

photoanodes	Electrolyte	Performance	References
$WO_3/BiVO_4/ZnO$	0.5 M Na_2SO_4	2.96 mA/cm^2 at 1.23 V vs RHE	1
$BiVO_4/rGO/Co_3O_4$	0.5 M Na_2SO_4	1.8 mA/cm^2 at 1.23 V vs RHE	2
BiVO4/NiO/rGO	0.5 M Na_2SO_4	1.52 mA/cm^2 at 1.23 V vs RHE	3
$BiVO_4$/NiFeOOH/Co-Pi	0.5 M Na_2SO_4	2.03 mA/cm^2 at 1.23 V vs RHE	4
$BiVO_4/TiO_2/NiCo_2O_4$	0.5 M Na_2SO_4	2.47 mA/cm^2 at 1.23 V vs RHE	5
$BiVO_4$/BNNPs/CoCr-LDH	0.1 M Na_2SO_4	3.8 mA/cm^2 at 1.23 V vs RHE	6
$BiVO_4/Bi_2S_3/NiCoO_2$	0.5 M Na_2SO_4	2.58 mA/cm^2 at 1.23 V vs RHE	7
$NiCoO_x$/Fe-g-$C_3N_4/BiVO_4$	0.5 M phos- phate buffer solution	5.34 mA/cm^2 at 1.23 V vs RHE	8
$BiVO_4$/N:$NiFeO_x$	0.5 M K_3BO_3 (pH = 9.5)	6.4 mA/cm^2 at 1.23 V vs RHE	9
$NiFeCoO_x$/CPF-TCB/Mo:$BiVO_4$	1 M potassium borate buffer (pH = 9.5)	6.66 mA/cm^2 at 1.23 V vs RHE	10
$Co_2AlO_4/MgO/BiVO_4$	0.5 M Na_2SO_4	3.52 mA/cm^2 at 1.23 V vs RHE	This work

References

1. Z. Ma, K. Song, L. Wang, F. Gao, B. Tang, H. Hou and W. Yang, *ACS Appl Mater Interfaces*, 2019, **11**, 889-897.
2. N. D. Quang, S. Majumder, P. C. Van, J.-R. Jeong, C. Kim and D. Kim, *Electrochimica Acta*, 2020, **364**.
3. S. Bai, J. Han, K. Zhang, Y. Zhao, R. Luo, D. Li and A. Chen, *International Journal of Hydrogen Energy*, 2022, **47**, 4375-4385.
4. G. Fang, Z. Liu and C. Han, *Applied Surface Science*, 2020, **515**.
5. S. S. M. Bhat, S. A. Lee, T. H. Lee, C. Kim, J. Park, T.-W. Lee, S. Y. Kim and H. W. Jang, *ACS Applied Energy Materials*, 2020, **3**, 5646-5656.
6. M. K. Mohanta, T. K. Sahu, S. Bhowmick and M. Qureshi, *Electrochimica Acta*, 2022, **415**.
7. S. Majumder, M. Gu and K. Hyeon Kim, *Applied Surface Science*, 2022, **574**.
8. Z. Liang, M. Li, K. H. Ye, T. Tang, Z. Lin, Y. Zheng, Y. Huang, H. Ji and S. Zhang, *Carbon Energy*, 2023, **413**.
9. B. Zhang, S. Yu, Y. Dai, X. Huang, L. Chou, G. Lu, G. Dong and Y. Bi, *Nature Communications*, 2021, **12**.
10. J. W. Yang, S. G. Ji, C.-S. Jeong, J. Kim, H. R. Kwon, T. H. Lee, S. A. Lee, W. S. Cheon, S. Lee, H. Lee, M. S. Kwon, J. Moon, J. Y. Kim and H. W. Jang, *Energy & Environmental Science*, 2024,**17**,2541.